

# Elastic-strain tensor by Rietveld refinement of diffraction measurements

Davor Balzar<sup>a)</sup>

*Materials Science and Engineering Laboratory, National Institute of Standards and Technology,  
325 Broadway, Boulder, Colorado 80303*

Robert B. Von Dreele and Kristin Bennett

*Manuel Lujan Jr. Neutron Scattering Center, Los Alamos National Laboratory, Los Alamos,  
New Mexico 87545*

Hassel Ledbetter

*Materials Science and Engineering Laboratory, National Institute of Standards and Technology,  
325 Broadway, Boulder, Colorado 80303*

(Received 20 February 1998; accepted for publication 13 July 1998)

A procedure to obtain all components of the elastic-strain tensor by simultaneous Rietveld refinement of diffraction patterns collected at different specimen orientations is described. The refined lattice parameters yield the hydrostatic strain component. If the lattice constants of the unstrained reference specimen are not known, the deviatoric strain tensor can still be determined. An anisotropic strain component may be refined for cubic and hexagonal crystal structures along with the isotropic. The method is applied to Al/SiC (short whisker) composites and systematic errors are assessed. © 1998 American Institute of Physics. [S0021-8979(98)00320-X]

## I. INTRODUCTION

Residual strains and associated stresses play a decisive role in materials properties. There are different methods of stress/strain determination, such as mechanical, acoustical, magnetical, optical, and diffraction. The diffraction method of measuring strain is limited to crystalline materials because it relies on the determination of interplanar  $d$  spacing. However, it is the most reliable and widely applicable method. X-ray diffraction was used in stress determination since 1925.<sup>1</sup> The strain is generally anisotropic and the diffraction method relies on measuring the interplanar  $d$  spacing along different directions in the laboratory coordinate system, using the so-called  $\sin^2 \psi$  method,<sup>2</sup> where  $\psi$  denotes the angle between the specimen-surface normal and the diffraction vector (Fig. 1). For the usual x-ray experimental setup (reflection geometry) and specimen geometry ("infinitely" thick for x-ray energies routinely used), large  $\psi$  tilts are not accessible. Regularly, this method is used with monochromatic x-ray or neutron beams. Because of weaker interaction with matter than x-rays, neutrons penetrate much more (typical penetration depth for x rays is of the order of  $\mu\text{m}$  but of the order of cm for neutrons). Therefore, neutron diffraction allows for a determination of bulk values nondestructively and all  $\psi$  tilts are accessible.

There are advantages in using a polychromatic neutron beam, such as obtained at spallation time-of-flight (TOF) neutron sources.<sup>3</sup> At every specimen orientation, the whole diffraction pattern is collected, thus yielding information on all available Bragg reflections. This is a big advantage especially in cases of strong texture, such as oriented fibers or whiskers, where the  $\sin^2 \psi$  method cannot be used with one diffraction line. A natural step forward is to use the complete

information contained in the diffraction pattern instead of using only one diffraction line. Among the full diffraction powder pattern fitting approaches, the Rietveld refinement<sup>4</sup> was developed into a powerful procedure to obtain a variety of information about the specimen.<sup>5</sup> Recently, the speedy texture determination by Rietveld refinement from relatively few specimen orientations was envisioned either by a two-step iterative approach<sup>6</sup> or by simultaneous refinement of texture harmonic coefficients<sup>7</sup> along with other refinable parameters in the Rietveld program.<sup>8</sup> Ferrari and Lutterotti<sup>9</sup> presented a Rietveld-refinement method for simultaneous determination of residual stresses and texture by x-ray diffraction. Residual stress was estimated from elastic strains and texture in a one-phase material by making particular assumptions on the properties of the stress-concentration tensor, which depends on specimen physical and crystal symmetries. The aim here is to present a simple method to obtain the complete elastic-strain tensor because the strain is directly measured by diffraction line shift. We opted to omit a path to the stress estimation in the Rietveld code because of potential complexity (especially because of possible low crystal and specimen symmetries, texture, multiphase materials, sharp strain gradients, etc.) of estimating stresses from strains. However, the texture harmonic coefficients are determined from the same set of measurements,<sup>8</sup> which allows calculations of orientation distribution function (ODF) and consequent weighting of monocrystal elastic constants and estimations of elastic stresses. These results will be presented elsewhere.<sup>10</sup> Therefore, all the strain and texture parameters can be obtained along with structural, microstructural, compositional, and other information for all the crystalline phases. We tested the method on often-studied Al/SiC (short whisker) composites. This approach also applies to x-ray and constant-wavelength neutron data, and even for data collected in a limited region (few peaks or even a single peak),

<sup>a)</sup>Electronic mail: balzar@boulder.nist.gov

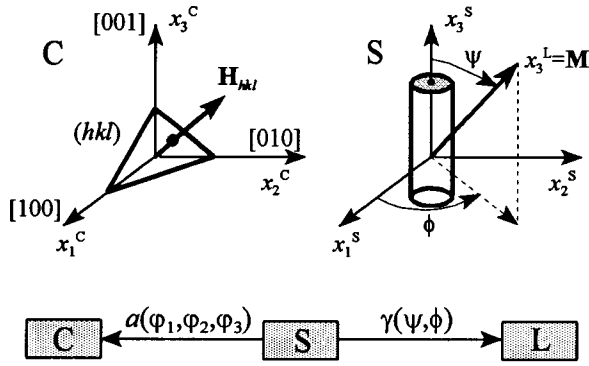


FIG. 1. Coordinate systems and transformation matrices used: Specimen system  $S$ , laboratory (measurement) system  $L$ , crystal system,  $C$ .  $x_1^L$  and  $x_2^L$  were not drawn for clarity.

but it is particularly suitable for TOF neutron-diffraction measurements where the whole pattern is collected simultaneously.

### II. RIETVELD-REFINEMENT CODING

As a general reference to the Rietveld refinement program, which is a part of the General Structure Analysis System (GSAS), the reader is directed to the original manual.<sup>11</sup> Here, only the specifics about strain-related coding in the Rietveld-refinement program will be given. The calculated intensity  $I_c$  of TOF diffraction data is given as

$$I_c = I_b + S_h \sum_p S_{ph} I_{ph}. \quad (1)$$

Here, indexes  $p$  and  $h$  extend over phases and histograms (patterns) in the experiment, respectively,  $I_b$  is the background intensity,  $S_h$  is the histogram scale factor,  $S_{ph}$  is the histogram-specific phase scale factor, and  $I_{ph}$  is the Bragg-intensity contribution from the  $h$ th reflection of the  $p$ th phase:

$$I_{ph} = F_{ph}^2 K_{ph} P(\Delta T_{ph}). \quad (2)$$

Here,  $F_{ph}$  denotes a structure factor,  $K_{ph}$  is the product of numerous correction factors,  $P$  is a diffraction-line profile function expressed in terms of TOF  $\Delta T_{ph}$ . The expected Bragg diffraction-line maximum position  $T_{ph}$  is determined from the  $d$  spacing as

$$T_{ph} = C_C d_p + C_A d_p^2 + C_0. \quad (3)$$

The constants  $C_C$ ,  $C_A$ , and  $C_0$  are characteristic for a particular counter bank on a TOF diffractometer.

Strain  $\epsilon_{ph,i}$  can cause the TOF shift from the diffraction-line maximum:

$$\Delta T_{ph} = (T - T_{ph}) - \epsilon_{ph,i} d_p. \quad (4)$$

Here,  $T$  extends over each diffraction-line point.

### III. METHODOLOGY

We define three coordinate systems:<sup>12</sup> specimen ( $\mathbf{x}_i^S$ ), crystal ( $\mathbf{x}_i^C$ ), and measurement ( $\mathbf{x}_i^L$ ), with transformation matrices as defined in Fig. 1. Index  $i$  extends over three axes

in the Cartesian system and throughout the paper the Einstein summation convention is assumed. The crystal system is conveniently chosen to coincide with principal crystal directions  $[100]$ ,  $[010]$ , and  $[001]$ . The direction of reciprocal-lattice vector  $\mathbf{H}_{hkl}$  of an  $(hkl)$  crystal plane in the crystal system is fixed by polar angle  $\eta$  and azimuthal angle  $\rho$ . The direction-cosine terms between  $\mathbf{H}_{hkl}$  and principal crystal directions are:

$$\beta_i = \begin{pmatrix} \sin \eta \cos \rho \\ \sin \eta \sin \rho \\ \cos \eta \end{pmatrix}, \quad (5)$$

and can be calculated from the unit-cell parameters and Miller indices  $hkl$  for all crystal classes.

Orientation of the crystal system relative to the specimen system

$$\mathbf{x}_i^C = a_{ij} \mathbf{x}_j^S \quad (6)$$

is fixed by three Euler angles,  $\varphi_1, \varphi_2, \varphi_3$ ,<sup>13</sup> which defines the transformation matrix as follows:<sup>14</sup>

$$a_{ij} = (\varphi_1)_{ik} (\varphi_2)_{kl} (\varphi_3)_{lj}. \quad (7)$$

Measurement at a particular diffracting angle is along the  $\mathbf{M}$  (diffraction vector) that must coincide with a reciprocal lattice vector  $\mathbf{H}_{hkl}$  for an  $(hkl)$  set of planes to diffract. Because all the crystal planes with parallel  $\mathbf{H}_{hkl}$  diffract, measured interplanar spacing  $d$  is invariant to the rotation around the direction of  $\mathbf{H}_{hkl}$  ( $\mathbf{H}_{hkl} \parallel \mathbf{M}$ , which is not fixed in the plane perpendicular to it), and polar angle  $\psi$  and azimuthal angle  $\phi$  suffice to define the matrix  $\gamma$ :

$$\mathbf{x}_i^L = \gamma_{ij} \mathbf{x}_j^S, \quad (8)$$

where

$$\gamma_{ij} = \psi_{ik} \phi_{kj}, \quad (9)$$

and, if  $\mathbf{M} \parallel x_3^L$  is chosen, this defines the direction-cosine matrix as

$$\gamma_{ij} = \begin{pmatrix} \cos \phi \cos \psi & \sin \phi \cos \psi & -\sin \psi \\ -\sin \phi & \cos \phi & 0 \\ \cos \phi \sin \psi & \sin \phi \sin \psi & \cos \psi \end{pmatrix}. \quad (10)$$

Therefore, the interplanar spacing (accordingly the strain obtained by diffraction methods) is averaged over an angle  $\omega$  around  $\mathbf{M}$  over all crystallites oriented favorably for diffraction:

$$\langle d_{\psi\phi} \rangle = \frac{\int_0^{2\pi} d\omega d_{33}^L f(g)}{\int_0^{2\pi} d\omega f(g)}. \quad (11)$$

Brackets indicate averaging over grains oriented favorably for diffraction in the whole diffracting volume and the average is weighted by the ODF  $f(g)$ , which is proportional to the grain volume fraction  $dV$  with the orientation  $g$  [defined by Euler angles in Eq. (7)]

$$f(g) = \frac{dV/V}{dg}. \quad (12)$$

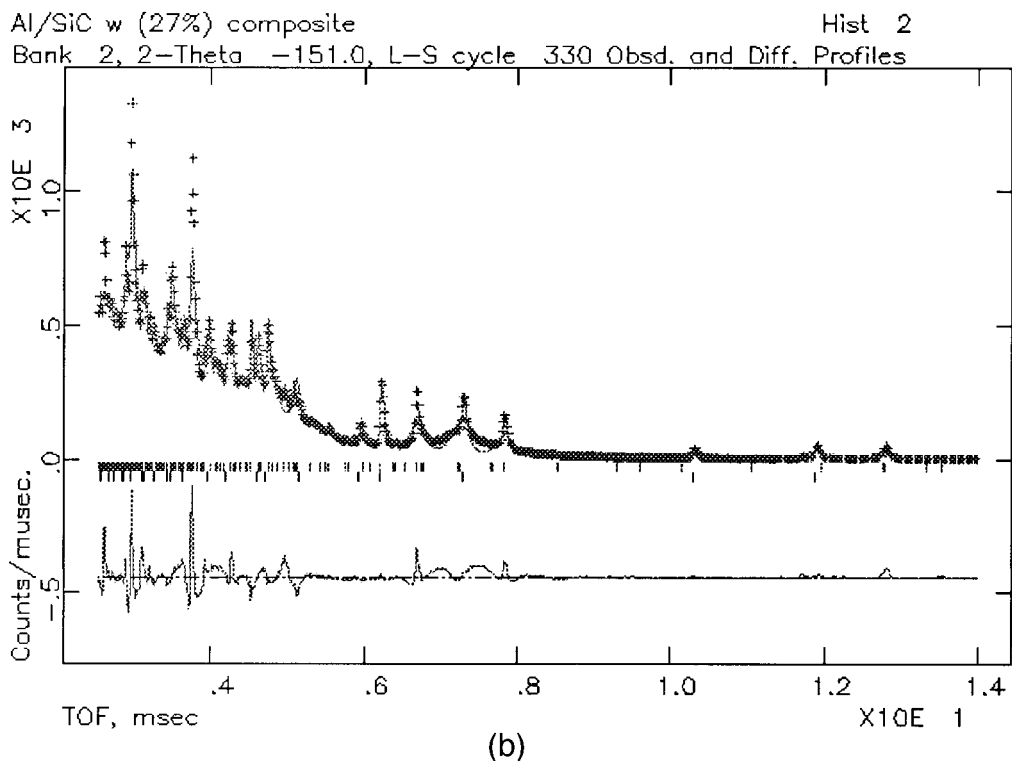
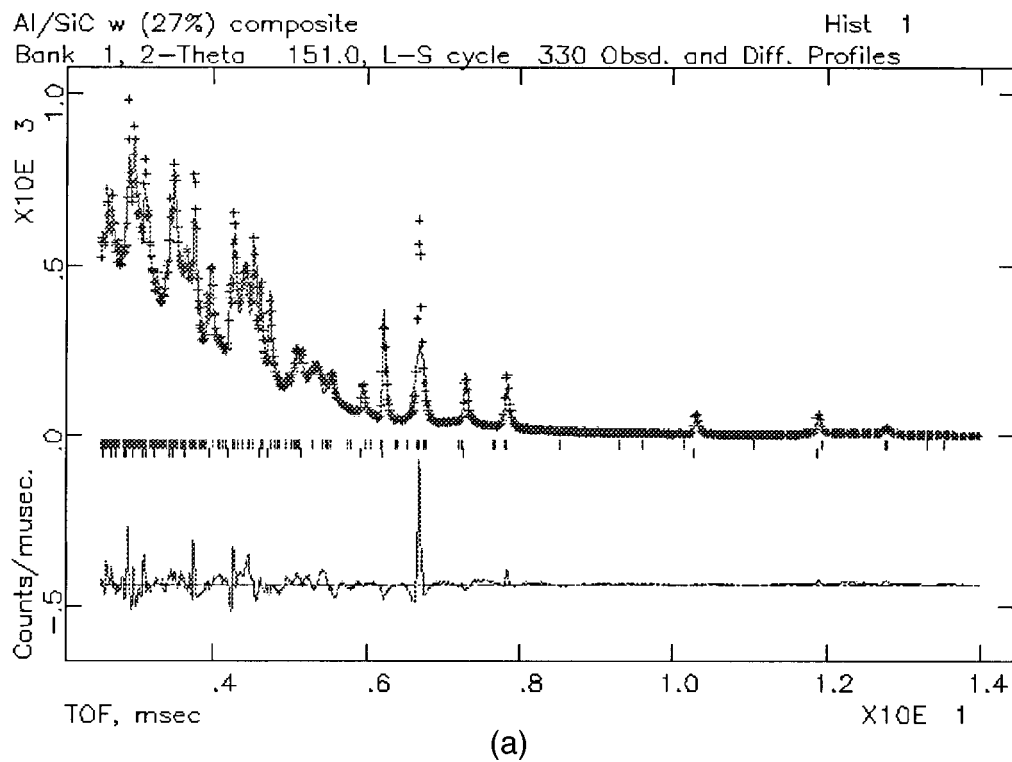


FIG. 2. Observed and refined by Rietveld refinement time-of-flight (TOF) diffraction patterns of Al-6061/27.9 vol % SiC composite collected at one of the 18 specimen orientations as seen with: (a)  $153^\circ$  data bank, (b)  $-153^\circ$  data bank, (c)  $90^\circ$  data bank, and (d)  $-90^\circ$  data bank.

#### IV. INTERPRETATION OF STRAIN-RELATED PARAMETERS IN THE RIETVELD PROGRAM

Because the TOF measurements already compile the whole diffraction pattern of each phase at all specimen orientations, strain can be estimated either from the particular  $d$  spacings of interest or from the refined lattice parameters. In

cases of strong texture, strain from the  $d$  spacing is difficult to measure because the diffracted Bragg intensity changes abruptly and is very small in particular directions (see Fig. 2). Furthermore, the latter is a more convenient approach because it is a part of the Rietveld-refinement procedure. However, lattice parameters yield an average measure of

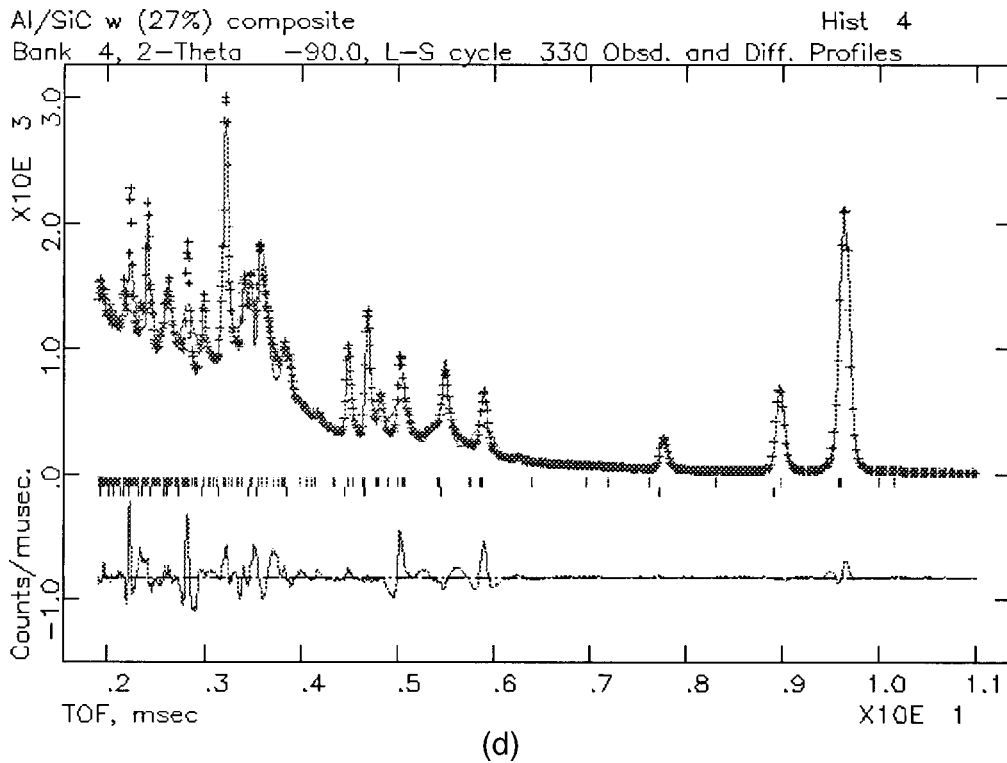
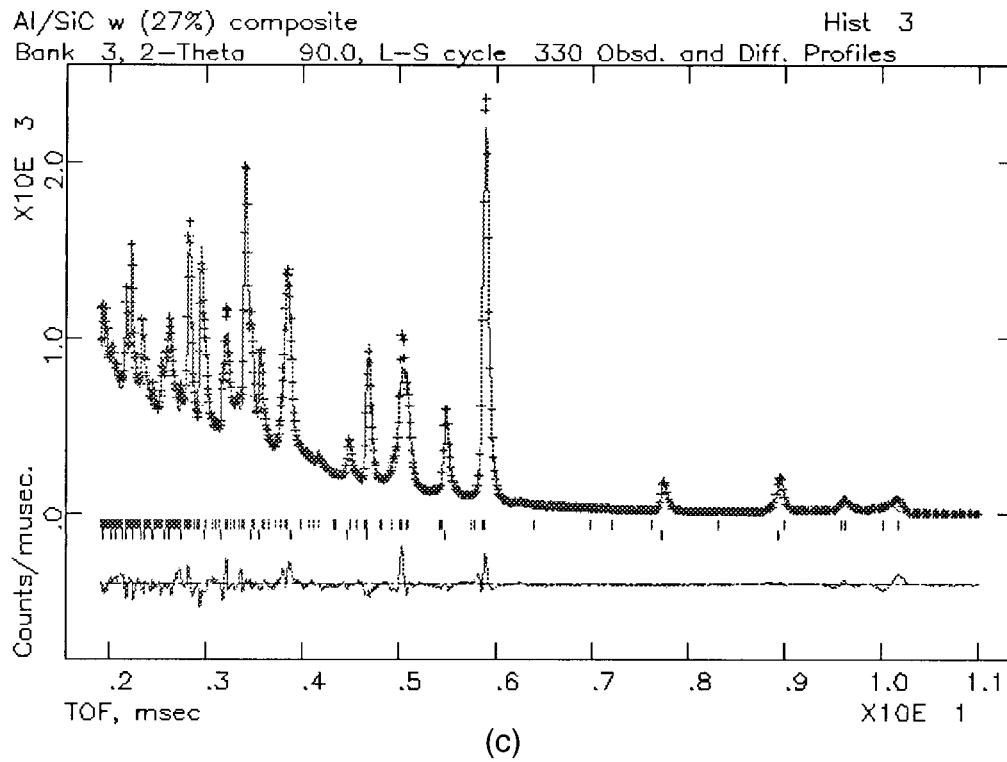


FIG. 2. (Continued.)

strain. It is important to understand the mutual relationship of all the parameters that relate to strain in Rietveld refinement through Eq. (4).

Strain parallel to  $x_3^L$  is calculated from a histogram-specific  $\langle d_{\psi\phi} \rangle$  that is measured along  $x_3^L$  at the specimen orientation  $\psi, \phi$ :

$$e_{\psi\phi} = \frac{\langle d_{\psi\phi} \rangle}{d_{p0}} - 1, \tag{13}$$

where  $d_{p0}$  is the unstrained (reference) interplanar spacing. The lattice parameters (which are adjusted in the least-squares refinement) are in the Rietveld program determined

from  $d_p$  spacings of allowed diffraction lines. The  $d_p$  spacing is averaged over all the specimen orientations, each having a histogram-specific  $\langle d_{\psi\phi} \rangle$ . For a sufficiently large number of collected histograms, evenly distributed over the specimen orientation angles  $\psi$  and  $\phi$ , summation can be replaced by integration over angles:

$$\langle d_p \rangle = \frac{1}{4\pi} \int_0^\pi d\psi \sin \psi \int_0^{2\pi} d\phi \langle d_{\psi\phi} \rangle. \quad (14)$$

For quasi-isotropic polycrystalline materials (that is, with a random orientation of crystallites),<sup>15</sup> by using Eqs. (8), (10), (11), and (13), the integral (14) follows as:

$$\frac{\langle d_p \rangle}{d_{p0}} - 1 \equiv \langle e \rangle = \frac{e_{11} + e_{22} + e_{33}}{3}. \quad (15)$$

The total strain can be divided in hydrostatic  $e^H$  and deviatoric components  $e'_{ij}$ :

$$e_{ij} = e'_{ij} + \delta_{ij} e^H, \quad (16)$$

where  $\delta_{ij}$  denotes the Kronecker  $\delta$  symbol. It follows:

$$e_{\psi\phi} \equiv \langle e_{33}^L \rangle = \gamma_{3k} \gamma_{3l} e_{kl} = e^H + \gamma_{3k} \gamma_{3l} e'_{kl}, \quad (17)$$

because of the orthogonality of coefficients

$$\gamma_{ik} \gamma_{kj} = \delta_{ij}. \quad (18)$$

The absolute magnitude of the refined parameter  $\epsilon_{ph,i}$  depends on the  $d_p$  spacing, as can be seen from Eqs. (3) and (4). Hence, there are two possibilities:

(i) Lattice parameters are refined together with other parameters: Then  $\langle d_p \rangle$  yields an average hydrostatic (direction-independent) component of strain, provided that the unstressed  $d_0$  for a reference specimen was determined:

$$\langle e \rangle = \text{Tr}(e_{ij})/3 \equiv e^H. \quad (19)$$

The refined parameters  $\epsilon_{ph,i}$  directly yield a deviatoric strain tensor. Note that the unstressed lattice spacing  $d_0$  is required solely to calculate the hydrostatic component of strain.<sup>16</sup> If it cannot be determined accurately, as it is often the case of triaxial stress,<sup>17</sup> the deviatoric strain tensor can still be obtained.

(ii) Lattice parameters are held constant at the previously determined value for the unstrained (reference) specimen: Then from Eq. (15) it follows that:

$$\text{Tr}(e'_{ij}) = 0. \quad (20)$$

This is also required by Eq. (16). The refined  $\epsilon_{ph,i}$  yields the complete strain tensor.

The difference in strain-tensor traces under (i) and (ii) therefore yields the hydrostatic strain component. Hence,  $\epsilon_{ph,i}$  for each phase and histogram, collected at particular specimen orientation angles  $\psi$  and  $\phi$ , is refined simultaneously during the Rietveld refinement. The strain components in the laboratory system  $\langle e_{33}^L \rangle \equiv e_{\psi\phi}$  follow from  $\epsilon_{ph,i}$  by correction for diffractometer constants [compare to Eq. (3)]. From Eqs. (8) and (10),

$$e_{\psi\phi} = e_{33} + (e_{11} \cos^2 \phi + e_{12} \sin 2\phi + e_{22} \sin^2 \phi - e_{33}) \times \sin^2 \psi + (e_{13} \cos \phi + e_{23} \sin \phi) \sin 2\psi. \quad (21)$$

Equation (21) can be solved simultaneously to yield the strain components in the specimen coordinate system.<sup>16,18</sup> The strain tensor is symmetric, so it has six independent components, and measurements for at least six independent specimen positions are required. It is advantageous, however, to collect data at as many specimen orientations as feasible. Moreover, because this approach is used to determine the texture simultaneously with other parameters in Rietveld refinement, the same measurements are used for strain determination.

The  $e_{\psi\phi}$  in the Rietveld refinement can often be an ‘‘average’’ value for the whole histogram, which may not be satisfactory in cases of significant crystalline anisotropy. Anisotropic corrections are treated later in the article (see Sec. VI). Alternatively, only a limited number of strain-related parameters in a small region (a vicinity around one diffraction line of interest) of every histogram can be refined. Thus, the  $e_{\psi\phi}$  will relate to only one Bragg reflection  $hkl$  and strains determined by Eq. (21) will be perpendicular to  $\{hkl\}$ .

A common experimental setup at TOF neutron sources for strain measurements is to orient the preferred symmetry axis of the specimen (for instance, cylinder axis of extruded composite materials) at an angle of 45° to the incident beam. Then, the  $\pm 90^\circ$  detector banks collect  $d$  spacings normal (radial-strain component) and parallel (axial-strain component) to the symmetry axis simultaneously. In cases of cylindrical specimen symmetry it is expected that these two components of strain suffice to describe the state of strain completely. However, we shall see in Sec. V that this may not be a satisfactory approximation. In any case, more than two specimen orientations yield the results with substantially higher precision and the complete state of strain tensor, as well as full texture information.

## V. EXAMPLES AND DISCUSSION

To illustrate this method we compare it with the more familiar and evident  $\sin^2 \psi$  approach. The material considered is an extruded Al-6061 alloy reinforced with SiC (hexagonal) whiskers (27.9 vol %). Details about specimen preparation are given elsewhere.<sup>19</sup> Figure 3 shows the microstructure, where extrusion of the monocrystal SiC whiskers orient preferably along the rod (extrusion) axis.

The measurements were obtained by a high intensity powder diffractometer (HIPD) at the Manuel Lujan Jr. Neutron Scattering Center (MLNSC), Los Alamos National Laboratory (Fig. 2). Throughout the article, it is assumed that  $x_3^S$  is along the specimen rod axis and measurements are done along the  $x_3^L$ . The measurements were collected at 18 different specimen positions (each defined by a set of  $\psi$  and  $\phi$  angles)<sup>8</sup> and only the measurements from high-angle detector banks ( $\pm 90^\circ$  and  $\pm 153^\circ$ ) were used in the Rietveld refinement to obtain a desired resolution. This gives an overdetermined system of 72 equations [Eq. (21)] that can be solved by least squares to obtain the complete strain tensor, thus minimizing the errors significantly. In principle, fewer measurements are needed to determine the strain tensor with sufficient precision. However, because the same set of measurements is used for texture determination, the optimum number

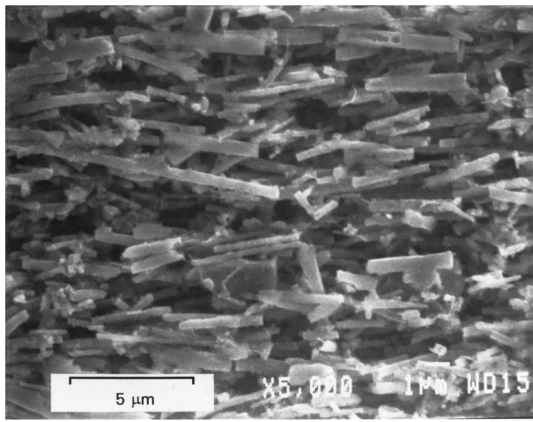


FIG. 3. Microstructure of Al-6061/27.9 vol % SiC composite. Rod-like SiC hexagonal monocrystals (0.05–1.5 μm in diameter with the volume-averaged aspect ratio of 7.4) align preferentially along the extrusion direction.

of specimen orientations will depend mainly on texture severity. To obtain the complete information on texture without *a priori* symmetry constraints, the measurements were made in the full azimuthal range,  $0^\circ \leq \phi < 360^\circ$ . Therefore, to detect the “ $\psi$  splitting”<sup>20</sup> in Eq. (21), it is not necessary to make measurements for both  $\psi < 0$  and  $\psi > 0$ , because the measurements at  $\psi > 0$  only and for  $\phi$  and  $\phi + 180^\circ$  give the same information<sup>21</sup> (both  $\sin \phi$  and  $\cos \phi$  change sign).

Rietveld refinement was carried out on full diffraction patterns (all the allowed Bragg diffraction lines with the interplanar spacing  $d > 0.5 \text{ \AA}$  were included) for all the  $\pm 90^\circ$  and  $\pm 153^\circ$  histograms that were collected at 18 different specimen orientations simultaneously. In our case (18 orientations  $\times$  4 histograms = 72 histograms), in the final cycles, that means 1743 refined parameters with 63 018 data points. No diffraction lines of SiC cubic (3C) polytype were identified. A 6H hexagonal structure was assumed and atomic positions of Si and C were fixed, but isotropic temperature factors were refined. Other refined parameters included scale factors, diffractometer constants, lattice parameters, relative crystal-phase fractions, absorption, texture, profile, and background coefficients. The initial specimen orientation angles, which may not coincide exactly with the assumed specimen coordinate system, were refined on the assumption of cylindrical specimen symmetry.<sup>8</sup> In the refinements, the measurements from the  $-90^\circ$  data bank were offset for a constant amount consistently at each specimen orientation. After attempts to refine the diffractometer constants for this particular data bank were unsuccessful (probably because of exact correlation of  $C_C$  with strain parameter  $\epsilon_{ph,i}$ ) these measurements were dropped from the subsequent analysis. This particular data bank gives information in the region  $0 \leq \sin^2 \psi < 0.15$ , that is, the range already covered with the  $-153^\circ$  detector bank for our experimental setup. Furthermore, strain parameters for the SiC phase only for histograms with  $\psi < 13^\circ$  were erratic with very large standard uncertainties and correlated strongly with the absorption parameters. We explain this by microabsorption effects because of the geometry and orientation of whiskers. These measurements were also dropped from the analysis.

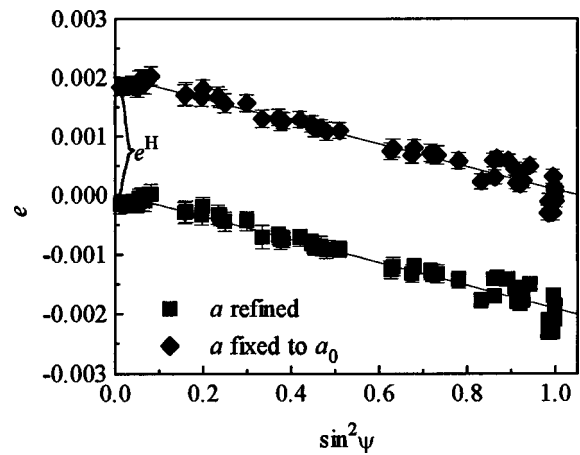


FIG. 4. Strain as a function of  $\sin^2 \psi$  in the Al-6061 matrix obtained from Rietveld refinements with lattice parameters both refined and fixed to the values of reference specimen.

The final refined strain parameters for all  $\psi$  and  $\phi$  pairs are plotted in Fig. 4 for the Al-6061 matrix for both cases described: (i) when the lattice parameter is refined; (ii) when the lattice parameter is fixed to the value of the reference specimen. Figure 5 gives pole figures, which were determined from the same set of histograms by Rietveld refinement, for both the Al-6061 matrix and the SiC whiskers. The approximate cylindrical symmetry around the specimen extrusion axis is evident for both phases. Then, strain is a function of polar angle only:

$$e(\psi) = \frac{1}{2\pi} \int_0^{2\pi} d\phi e_{\psi\phi}. \quad (22)$$

From Eq. (21), it immediately follows that

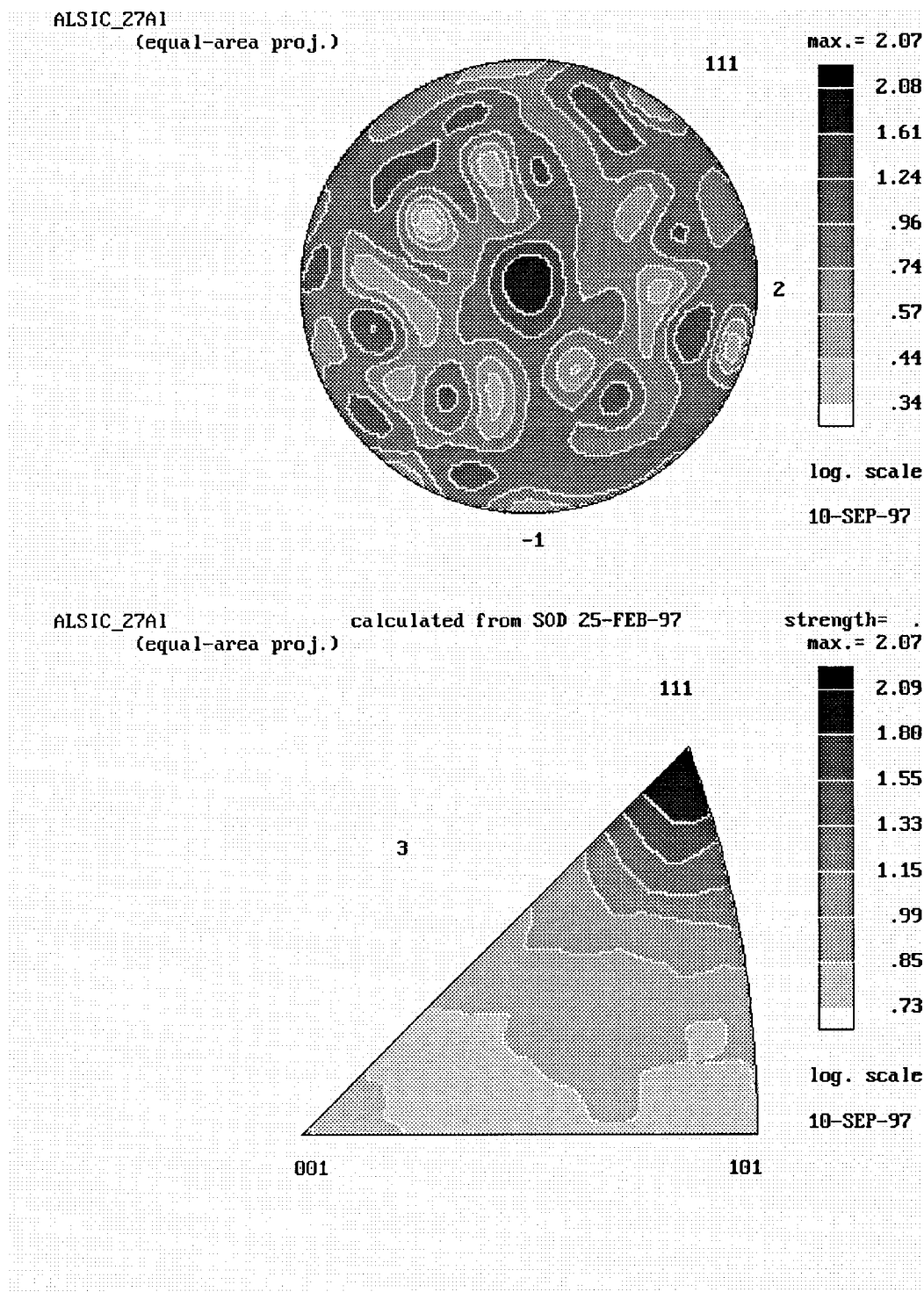
$$e(\psi) = e^H + e'_{33} + (e'_{11} - e'_{33}) \sin^2 \psi, \quad (23)$$

where it is assumed that

$$\frac{e'_{11} + e'_{22}}{2} \approx e'_{11} \quad (24)$$

because of cylindrical symmetry.

In this case, the  $\sin^2 \psi$  type analysis is performed easily and the linear fits were drawn through the points according to Eq. (23). The difference of ordinate intercepts directly yields  $e^H$ , whereas slopes must remain equal. Table I compares results of this approximate calculation with accurate results obtained by simultaneous solution of Eqs. (21), and Table II gives the complete strain tensors according to the latter method. Two radial components ( $e_{11}$  and  $e_{22}$ ) have similar values because of symmetry, as expected by Eq. (24). The total matrix strain is relatively small in the radial direction and given almost entirely by the hydrostatic component in the axial direction. The magnitude of strains is very sensitive to the choice of reference (standard) specimen because as-received Al 6061 powder, filings from the unreinforced, and reinforced alloy, are all different.<sup>22</sup> Some authors use different reference values in different directions, such as measured interplanar spacing of an unreinforced alloy parallel and perpendicular to the symmetry axis.<sup>23</sup> Tables I and II give strains relative to the unreinforced alloy filings, whose

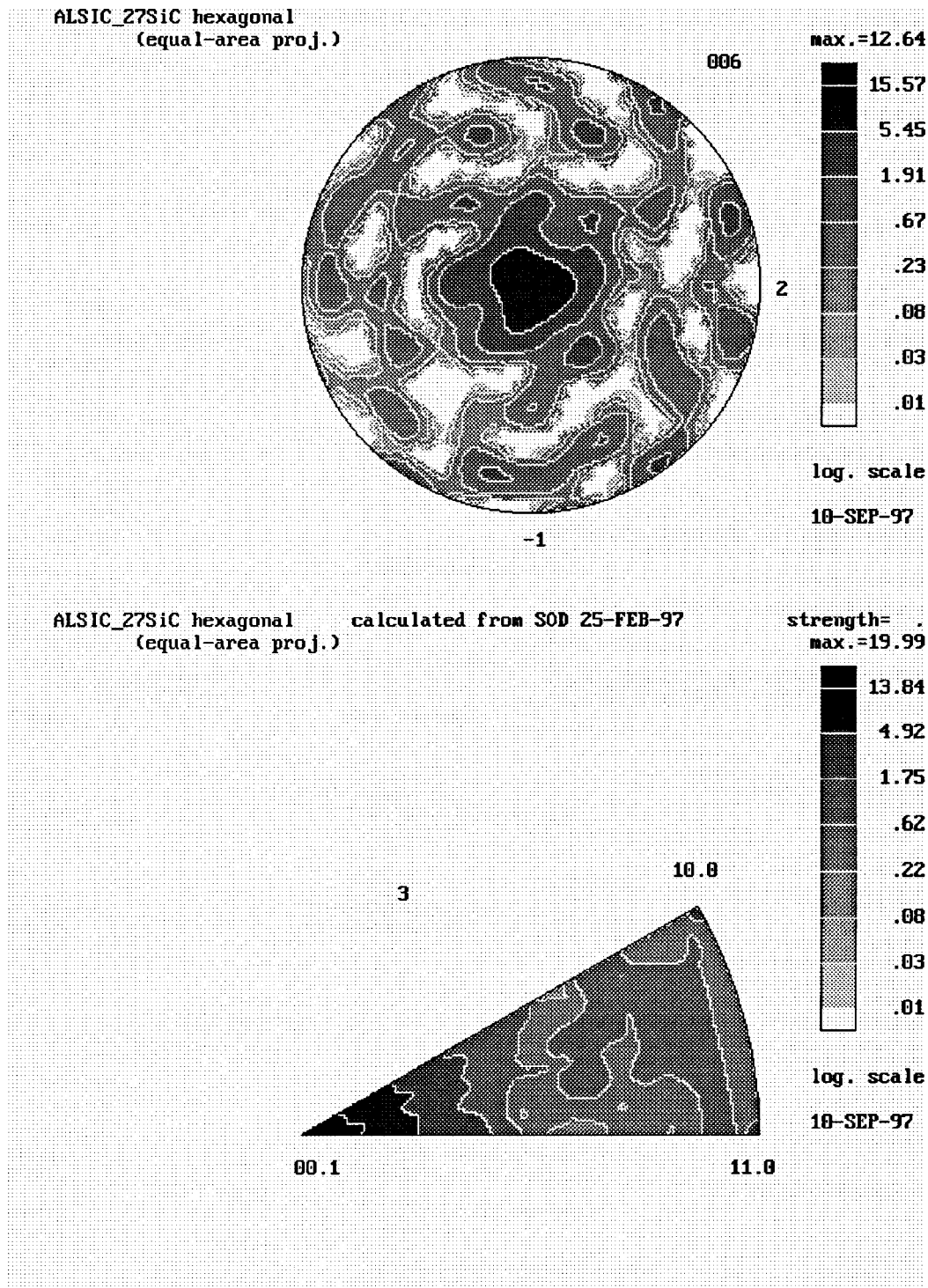


(a)

FIG. 5. Pole figures plotted in specimen axes and inverse pole figures plotted in crystal axes by the popLA program (see Ref. 41): (a) Al-6061 matrix, (b) SiC whiskers.

lattice parameter was determined as  $a = 4.0524(2)$  Å. Conversely, the lattice parameters of the bulk unreinforced alloy were  $a = 4.0478(4)$  Å in the radial direction (perpendicular to the specimen rod axis) and  $a = 4.0549(3)$  Å in the axial direction (parallel to the specimen rod axis). This gives an additional compression component of  $-1.14 \times 10^{-3}$  strain in the radial direction and a tension component of  $0.62 \times 10^{-3}$

strain in the axial direction of the bulk unreinforced alloy relative to the powder, which can be identified as a macrostrain caused by the extrusion. Therefore, the strains presented in Tables I and II are mainly thermally induced because of different coefficients of thermal expansion of matrix and reinforcement, but they also contain a contribution of macrostrain from the extrusion process. If the matrix strains from



(b)

FIG. 5. (Continued.)

Table II are corrected for the macrostrain component, in the radial direction there is a net tensile thermal strain of  $1.26 \times 10^{-3}$  and  $1.41 \times 10^{-3}$  in axial direction. The axial strain agrees fairly well with predicted values from finite-element modeling calculations<sup>23</sup> for thermally induced strain. However, despite relatively small anisotropy of the Al-6061 matrix, because of highly textured whisker reinforcements, a much smaller value for radial component is expected. The

possible reason for the discrepancy may be the unreliable measurement for the  $-90^\circ$  data bank, as explained above, and possible significant differences of unstressed lattice parameters between the unreinforced and reinforced Al-6061 alloy.<sup>22</sup>

Figure 6 and Tables I and II give the same results for the SiC phase. Because of a large SiC elastic stiffness and anisotropy, the hydrostatic strain component is relatively small

TABLE I. Diagonal components of deviatoric strain tensor of Al-6061 matrix and SiC whiskers obtained by a least-squares linear fit of data points in Figs. 4 and 6 and by the least-squares solution of system of Eq. (21). The hydrostatic component  $e_1^H$  was obtained as a difference in ordinate intercept (least-squares linear fit) or as the weighted average difference in diagonal components of the strain tensors (solution of system of equations) for two cases (lattice parameters refined and fixed to the lattice parameters of the reference specimens). The hydrostatic component  $e_2^H$  was obtained as a relative difference of the refined and reference lattice parameters. The unstrained (reference) lattice parameters were obtained by Rietveld refinement of the diffraction patterns of Al-6061 unreinforced-alloy filings and of SiC whiskers extracted from the composites.

Strain ( $10^{-3}$ )	Al		SiC	
	Linear fit	System of equations	Linear fit	System of equations
$e'_{11}$	...	-1.91(6)	...	-0.31(5)
$e'_{22}$	-1.91(10)	...	-0.19(8)	...
$e'_{33}$	...	-1.86(5)	...	-0.22(4)
$e_1^H$	0.03(4)	0.02(4)	0.84(7)	0.83(7)
$e_2^H$	2.00(8)	2.01(10)	-0.19(14)	-0.14(11)
	2.01(5)		-0.20(29)	
Lattice parameters (Å)	Composite specimen	Reference specimen	Composite specimen	Reference specimen
$a$	4.06055(1)	4.0524(2)	3.07907(1)	3.0794(5)
$c$	—	—	15.114(2)	15.120(6)

and could not be determined with sufficient precision (standard uncertainty is about 80%). However, the deviatoric strain component can still be determined with relatively high precision, which is usually not possible with other methods because of a strong SiC texture and especially in view of relatively low instrument resolution (HIPD has a relatively short flight path and estimated resolution  $\Delta d/d=0.3\%$  for the  $\pm 153^\circ$  data banks). Considering the macrostrain contribution, the SiC thermal-strain component appears to be zero in axial and tensile in radial direction. Although the latter was reported,<sup>23</sup> it is likely that the results are influenced by unreliable hydrostatic and radial macrostrain strain components. Table II also indicates that the shear-strain component  $e_{13}$  is significant, which explains the “ $\psi$  splitting” seen in Fig. 6; this information cannot be obtained by simplified measurements at  $\pm 90^\circ$ .

Proper care must be taken to minimize potentially serious systematic errors in strain determination because of inevitable specimen shifts off the goniometer symmetry axis during rotation. If the volume sampled by the beam (as defined by the cross section of incident and diffracted beams) is not entirely contained in the specimen (assumed to have a homogeneous strain distribution) at each specimen position, a small shift from the central position will be interpreted as strain [compare Eqs. (3) and (4)]. A qualitative indication of the magnitude of such error is scatter of individual values of strain around the mean, such as in Fig. 4. The error in strain is defined by the uncertainty in the measurement of lattice spacings, that is, the measured time of flight. The component of specimen displacement along the direction of the incident beam,  $\Delta x$ , equals:<sup>24</sup>

TABLE II. All the components of the total strain tensor obtained by a least-squares solution of the system of Eqs. (21) for both the Al-6061 and SiC phases.

Strain ( $10^{-3}$ )	Al	SiC
$e_{11}$	0.10(5)	-0.43(5)
$e_{22}$	0.13(5)	-0.33(4)
$e_{33}$	2.03(5)	0.64(7)
$e_{12}$	-0.13(4)	-0.10(4)
$e_{13}$	0.01(5)	0.17(6)
$e_{23}$	0.01(5)	0.02(6)

$$\frac{\Delta T}{T} = \frac{\Delta x}{2l_2} \cot \theta + \frac{\Delta x}{l}, \quad (25)$$

where  $l$  is the total and  $l_2$  is the scattered flight-path length. Equation (25) indicates that this error is smallest for the large Bragg angle  $\theta$ , which is confirmed by Fig. 4. As an estimate, the relative error of lattice parameters determined (from a single specimen orientation) at HIPD was about  $10^{-4}$ . This is equivalent to the shift of 0.2 mm for the  $\pm 90^\circ$  detector banks and to 0.5 mm for the  $\pm 153^\circ$  detector banks.

In our measurements, the specimen cylinder axis was kept in the diffractometer (horizontal) plane at angles between  $44^\circ$  and  $69^\circ$  to the forward-transmitted beam, while the specimen was rotated around cylinder axis for a full  $360^\circ$ . In this way, the  $-153^\circ$  detector banks yield strain in the range  $0 < \sin^2 \psi < 0.3$ , the  $153^\circ$  detector banks in the range  $0.3 < \sin^2 \psi < 0.8$ , and the  $90^\circ$  detector banks in the range  $0.8 < \sin^2 \psi < 1.0$ . Thus, the majority of data are collected at a large Bragg angle where systematic errors have the least effect. Figure 4 shows that the scatter around the mean value is independent of a particular detector bank, which indicates that the systematic errors of strains due to specimen displacement will be more serious if strain is determined from the measurement at one specimen orientation, such as with the  $\pm 90^\circ$  detector banks.

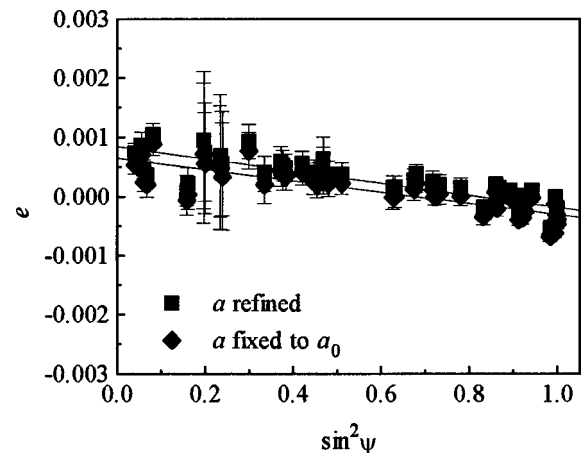


FIG. 6. Strain as a function of  $\sin^2 \psi$  in SiC whiskers obtained from Rietveld refinements with lattice parameters both refined and fixed to the values of reference specimen.

## VI. ANISOTROPIC STRAIN CORRECTIONS

Starting from the measured strains, it is always possible to calculate the strains in the specimen coordinates, according to Eq. (21). It is of interest to obtain the stresses in the same coordinate system. Elastic strain and stress tensors are related through Hooke's law:

$$\sigma_{ij}^C = c_{ijkl} e_{kl}^C; \quad e_{ij}^C = s_{ijkl} \sigma_{kl}^C, \quad (26)$$

where  $c_{ijkl}$  and  $s_{ijkl}$  are the single-crystal fourth-rank stiffness and compliance tensors, respectively. However, for a polycrystalline aggregate, the polycrystalline elastic constants have to be calculated or measured. They depend generally in a complicated way on the values of monocrystal elastic constants, texture and coupling of the grains. A linear relation between strain and stress can be established as:<sup>12,21</sup>

$$e_{\psi\phi} \equiv \langle e_{33}^L \rangle = R_{33ij}^L \sigma_{ij}^L = F_{ij}(\psi, \phi, hkl) \sigma_{ij}^S. \quad (27)$$

$R_{33ij}^L$  (fourth-rank tensor) and  $F_{ij}$  (coefficients) depend on the monocrystal compliances, texture, and elastic interactions between grains or phases. Because of their dependence on crystallographic direction,  $R_{33ij}^L$  are called diffraction compliances.<sup>25</sup> In the quasi-isotropic case, they become

$$R_{33ij}^L(hkl) = S_1(hkl) \delta_{ij} + \frac{1}{2} S_2(hkl) \delta_{3i} \delta_{3j}; \quad (28)$$

$$S_1(hkl) = -\frac{\nu}{E}; \quad \frac{1}{2} S_2(hkl) = \frac{1+\nu}{E},$$

where  $\nu$  is Poisson's ratio,  $E$  is Young's modulus, and  $S_1$  and  $S_2/2$  are termed diffraction elastic constants.<sup>25</sup> If constant stress in grains is assumed (Reuss<sup>26</sup> approximation), they follow for cubic crystal symmetry (in matrix notation) as:<sup>27,28</sup>

$$S_1(hkl) = s_{12} + s_0 \Gamma_C; \quad \frac{1}{2} S_2(hkl) = s_{11} - s_{12} - 3 \Gamma_C s_0;$$

$$s_0 = s_{11} - s_{12} - s_{44}/2. \quad (29)$$

Similar relations<sup>29</sup> follow in the case of the Kröner<sup>30</sup> approximation, whereas the Voigt<sup>31</sup> assumption (constant strain in grains) gives diffraction elastic constants independent of crystallographic direction (see, for instance, the review by Hauk<sup>32</sup>). Here,  $\Gamma_C$  is the orientation parameter for cubic crystals:

$$\Gamma_C = \beta_1^2 \beta_2^2 + \beta_2^2 \beta_3^2 + \beta_3^2 \beta_1^2 = \frac{h^2 k^2 + k^2 l^2 + l^2 h^2}{(h^2 + k^2 + l^2)^2}. \quad (30)$$

It varies from 0 for  $\{h00\}$  to 1/3 for  $\{hhh\}$ . Similarly, for hexagonal crystals one can define the parameter

$$\Gamma_H = \beta_3^2 = \frac{l^2}{\frac{4}{3} \frac{c^2}{a^2} (h^2 + hk + k^2) + l^2}, \quad (31)$$

which is zero for  $\{hk0\}$ . An anisotropic behavior of strains was found<sup>33</sup> for hexagonal  $\text{Si}_3\text{N}_4$  whiskers that can be approximately modeled by Eq. (31).

Therefore, for cubic and hexagonal materials, the anisotropic effect can be modeled by a single refinable parameter in Rietveld refinement. Analogous to Eq. (4), in addition to

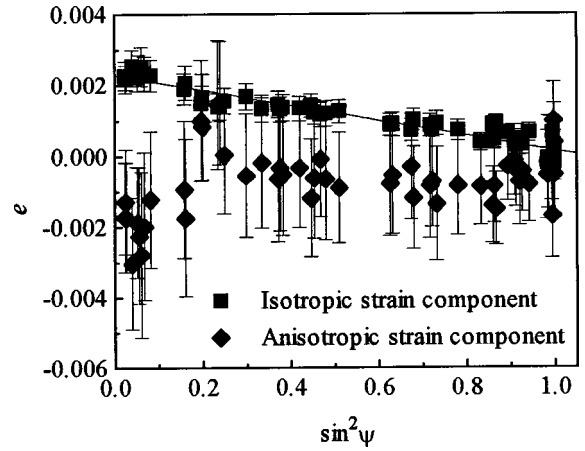


FIG. 7. Isotropic and anisotropic component of strain as a function of  $\sin^2 \psi$  in the Al-6061 matrix obtained from Rietveld refinements with lattice parameters fixed to the values of reference specimen.

the  $hkl$ -independent component  $i$  of strain  $\epsilon$ , the  $hkl$ -dependent component  $a$  is allowed to cause the TOF shift from the diffraction-line maximum:

$$\Delta T_{ph} = (T - T_{ph}) - \epsilon_{ph,i} d_p - \epsilon_{ph,a} d_p \Gamma. \quad (32)$$

Clearly, if a larger region of the diffraction pattern is refined, Eq. (32) should markedly improve the fit compared to Eq. (4). Moreover, the stresses can be estimated directly from  $\epsilon_{ph,i}$  and  $\epsilon_{ph,a}$  as follows: For cylindrical specimen symmetry, with

$$e_{ij} = S_2/2 \sigma_{ij} + \delta_{ij} S_1 \sigma_{kk}, \quad (33)$$

which is valid only in the quasi-isotropic case, under the Reuss hypothesis, Eq. (29), from Eq. (21) one gets the following relationships:

$$e_i = 3 s_{12} \sigma^H + (s_{11} - s_{12}) [\sigma_{33} + (\sigma_{11} - \sigma_{33}) \sin^2 \psi];$$

$$e_a = 3 s_0 [\sigma^H - \sigma_{33} - (\sigma_{11} - \sigma_{33}) \sin^2 \psi]. \quad (34)$$

Here,  $e_i$  and  $e_a$  follow directly from  $\epsilon_{ph,i}$  and  $\epsilon_{ph,a}$  by a division with the appropriate diffractometer constants, and hydrostatic stress  $\sigma^H$  is defined analogously as the hydrostatic strain in Eq. (19). From the strain parameters, two intercepts and slopes give the sought stress components. Equation (34) shows that slopes must have the opposite signs. Figures 7 and 8 present the results for the Al-6061 and SiC phases, respectively. The meaning of the  $e_i$  value is different from the strain presented in Figs. 4 and 6. The latter is strain averaged over all the  $\langle hkl \rangle$ , while the former presents the strain perpendicular to  $\{h00\}$  for cubic and  $\{hk0\}$  for hexagonal, according to its meaning in Eqs. (30), (31) and (32).<sup>34</sup>

For other than cubic or hexagonal crystal symmetries, two parameters are needed to model the  $hkl$  dependence.<sup>35</sup> Furthermore, for textured specimens, the orientation parameters  $\Gamma$  do not explicitly enter calculations of stresses, although it was found for some textured cubic materials that the elastic behavior in different crystal directions correlates with the orientation parameter  $\Gamma_C$ .<sup>12</sup>

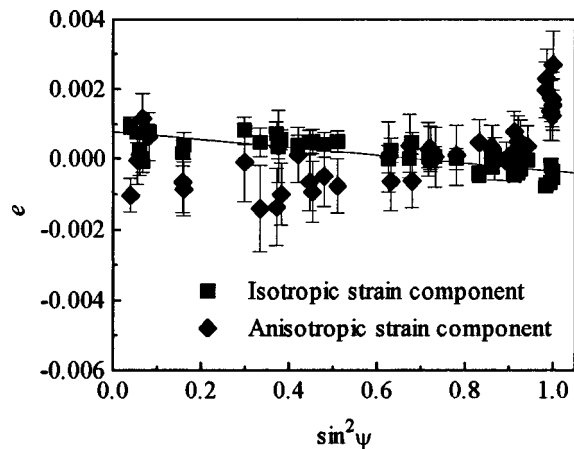


FIG. 8. Isotropic and anisotropic component of strain as a function of  $\sin^2 \psi$  in SiC whiskers obtained from Rietveld refinements with lattice parameters fixed to the values of reference specimen.

## VII. CONCLUSIONS

An approach to obtain all components of the elastic-strain tensor with a high precision from diffraction-line shifts is described. During the Rietveld refinement, strain-related parameters are adjusted together with other refinable parameters to fit multiple diffraction patterns (collected at different specimen orientations) simultaneously. From the same refinements, texture information, which can be used to calculate the accurate stress state from the strain tensor, is determined. The method is also applicable to x-ray or neutron constant-wavelength sources but is especially convenient with polychromatic sources, such as TOF neutrons.

The diffraction-line shift analysis of TOF neutron-diffraction measurements yields elastic strains/stresses that change across the scale of grain size (the II kind residual stresses), which makes this method very suitable to study multiphase composite materials or single-phase plastically deformed alloys where strains vary from grain to grain because of elastic incompatibilities of grains in a polycrystalline aggregate.<sup>36</sup> TOF neutron-diffraction measurements are usually accomplished with a relatively large beam cross section. The strain measurement thus obtained is averaged over a large specimen volume, which makes any interpretation of large strain gradients difficult to interpret. For instance, the strains that are balanced between macroscopic regions in the specimen (macrostrains or strains/stresses of the I kind due to machining, grinding, plastic deformation, and so on) will give diffraction-line shifts in different directions for different regions in the specimen. If the whole volume is sampled by the beam, there will be no effective diffraction-line shifts,<sup>37</sup> but this will be evident in diffraction-line broadening. Other localized inhomogeneous deformations associated with dislocations, point defects, and extended defects, such as stacking and twin faults, also contribute to the diffraction-line broadening.<sup>38</sup> These effects are usually summarized under the term residual stresses of the III kind and potentially provide complementary information to the stresses obtained from diffraction-line shifts. There were a few studies<sup>39,40</sup> published recently on this subject, although no generally ac-

cepted theory inclusive of all the mentioned microstructural effects currently exists. This is the object of current study.

## ACKNOWLEDGMENTS

The authors thank A. Winholtz (University of Missouri, Columbia) for providing the program which we adapted for strain calculations from TOF neutron data. This work has benefitted from the use of the Los Alamos Neutron Science Center at the Los Alamos National Laboratory. This facility is funded by the US Department of Energy under Contract No. W-7405-ENG-36.

<sup>1</sup>H. H. Lester and R. M. Aborn, *Army Ordnance* **6**, 120 (1925–26).

<sup>2</sup>H. Dölle and V. Hauk, *Härterei-Tech. Mitt.* **31**, 165 (1976).

<sup>3</sup>S. Majumdar, D. Kupperman, and J. Singh, *J. Am. Ceram. Soc.* **71**, 858 (1988).

<sup>4</sup>H. M. Rietveld, *J. Appl. Crystallogr.* **22**, 151 (1967).

<sup>5</sup>R. A. Young, Editor, *The Rietveld Method* (Oxford University Press, Oxford, 1993).

<sup>6</sup>S. Matthies, L. Lutterotti, and H. R. Wenk, *J. Appl. Crystallogr.* **30**, 31 (1997).

<sup>7</sup>H.-J. Bunge, *Texture Analysis in Materials Science* (Butterworth & Co., London, 1982).

<sup>8</sup>R. B. Von Dreele, *J. Appl. Crystallogr.* **30**, 517 (1997).

<sup>9</sup>M. Ferrari and L. Lutterotti, *J. Appl. Phys.* **76**, 7246 (1994).

<sup>10</sup>D. Balzar and H. Ledbetter (unpublished).

<sup>11</sup>A. C. Larson and R. B. Von Dreele, General Structure Analysis System GSAS, Los Alamos National Laboratory Report LAUR 86-748 (1986).

<sup>12</sup>M. Barral, J. L. Lebrun, J. M. Sprauel, and G. Maeder, *Metall. Trans. A* **18**, 1229 (1987).

<sup>13</sup>Different notations for three Euler angles are being used in the literature. We follow the Roe (Ref. 14) definition, but to avoid mixing of symbols, especially  $\psi$  and  $\phi$ , which are traditionally used to define the  $L \rightarrow S$  matrix of coefficients, the Euler angles are denoted as  $\theta = \varphi_1$ ,  $\psi = \varphi_2$ ,  $\phi = \varphi_3$ .

<sup>14</sup>R.-J. Roe, *J. Appl. Phys.* **36**, 2024 (1965).

<sup>15</sup>If texture exists, the measured interplanar spacing is weighted by the ODF and the general texture effects have to be considered carefully. Because the integration in Eq. (11) is around the normal to the diffracting plane, for crystal symmetries where elastic properties are isotropic in that plane (such as {111} cubic and {001} hexagonal), it is expected that texture has no effect if the sample symmetry axis coincides with that direction. This may explain why the  $\langle hhh \rangle$  strains of cubic materials do not show texture effects (Ref. 12). In the example given later in this study, Al matrix possesses a strong cylindrically symmetrical [111] texture and SiC hexagonal whiskers a strong [001] cylindrically symmetrical texture (compare to Fig. 5). Thus, the averaging over different  $\{hkl\}$  in Rietveld refinement will effectively favor these preferred orientations for each phase and texture effects on measured average strains will be negligible.

<sup>16</sup>R. A. Winholtz and J. B. Cohen, *Aust. J. Phys.* **41**, 189 (1988).

<sup>17</sup>I. C. Noyan and J. B. Cohen, *Residual Stress, Measurement by Diffraction and Interpretation* (Springer, New York, 1987).

<sup>18</sup>T. Imura, S. Weissmann, and J. J. Slade, Jr., *Acta Crystallogr.* **15**, 786 (1962).

<sup>19</sup>M. L. Dunn and H. Ledbetter, *Acta Mater.* **45**, 3327 (1997).

<sup>20</sup>If at least one shear strain ( $e_{13}$  or  $e_{23}$ ) is nonzero, the measured strain at a particular  $\phi$  will be different at  $\psi$  and  $-\psi$  according to Eq. (21). See in H. Dölle and V. Hauk, *Z. Metallkd.* **68**, 728 (1977).

<sup>21</sup>H. Dölle, *J. Appl. Crystallogr.* **12**, 489 (1979).

<sup>22</sup>R. J. Arsenault and A. D. Krawitz, *Residual Stresses in Composites; Measurement, Modeling & Effects on Thermo-Mechanical Behavior* (Minerals, Metals & Materials Society, Warrendale, PA, 1993), pp. 115–130.

<sup>23</sup>G. L. Povirk, M. G. Stout, M. Bourke, J. A. Goldstone, A. C. Lawson, M. Lovato, S. R. Macewen, S. R. Nutt, and A. Needleman, *Acta Metall. Mater.* **40**, 2391 (1992).

<sup>24</sup>J. D. Jorgensen, J. Faber, Jr., J. M. Carpenter, R. K. Crawford, J. R. Haumann, R. L. Hitterman, R. Kleb, G. E. Ostrowski, F. J. Rotella, and T. G. Worlton, *J. Appl. Crystallogr.* **22**, 321 (1989).

<sup>25</sup>The common terms are x-ray compliances and x-ray elastic constants, but they also are evidently valid for neutron diffraction.

<sup>26</sup>A. Reuss, *Z. Angew. Math. Mec.* **9**, 49 (1929).

- <sup>27</sup>R. Glocker, *Z. Tech. Phys. (Leipzig)* **19**, 289 (1938).
- <sup>28</sup>H. Möller and G. Martin, *Mitt. K. W. I. Eisen. Düsseldorf* **21**, 261 (1939).
- <sup>29</sup>F. Bollenrath, V. Hauk, and E. H. Müller, *Z. Metallkd.* **58**, 76 (1967).
- <sup>30</sup>E. Kröner, *Z. Phys.* **151**, 504 (1958).
- <sup>31</sup>W. Voigt, *Lehrbuch der Kristallphysik* (Teubner, Leipzig-Berlin, 1928).
- <sup>32</sup>V. Hauk, *Structural and Residual Stress Analysis by Nondestructive Methods* (Elsevier, Amsterdam, The Netherlands, 1997), p. 280.
- <sup>33</sup>S. Majumdar, J. P. Singh, D. Kupperman, and A. D. Krawitz, *J. Eng. Mater. Technol.* **113**, 51 (1991).
- <sup>34</sup>M. R. Daymond, M. A. M. Bourke, R. B. Von Dreele, B. Clausen, and T. Lorentzen, *J. Appl. Phys.* **82**, 1554 (1997).
- <sup>35</sup>In Ref. 32, p. 292.
- <sup>36</sup>S. R. MacEwen, J. Faber, Jr., and A. P. L. Turner, *Acta Metall.* **31**, 657 (1983).
- <sup>37</sup>This is for a sufficiently small specimen, so that the absorption can be neglected. Evidently, the origin of diffraction-line shifts will depend on the relative size of a specimen and the beam. If a specimen is completely bathed in the beam at any orientation, macrostrain should balance to zero, but there will be a more pronounced systematic error in strains because of specimen shifts. Conversely, macrostrain will be measurable, as shown earlier in the article.
- <sup>38</sup>B. E. Warren, *X-Ray Diffraction* (Addison-Wesley, Reading, MA, 1969), pp. 251–314.
- <sup>39</sup>R. I. Todd, C. Borsa, B. Derby, and M. A. M. Bourke, *Nucl. Instrum. Methods Phys. Res. A* **354**, 139 (1995).
- <sup>40</sup>C. M. Weisbrook, V. S. Gopalaratnam, and A. D. Krawitz, *Mater. Sci. Eng., A* **201**, 134 (1995).
- <sup>41</sup>J. S. Kallend, U. F. Kocks, A. D. Rollet, and H.-R. Wenk, *Mater. Sci. Eng., A* **132**, 1 (1991).